IRSTI 29.27.39; 29.27.47.

Plasma expansions in terms of self-similar solutions

M. Murakami

Institute of Laser Engineering, Osaka University, Osaka 565-0871, Japan
e-mail: murakami-m@ile.osaka-u.ac.jp

Simple analytical models are presented for hydrodynamic expansion of laser-produced plasma governed by the nonlinear heat conduction. To neatly describe the fluid systems, we put forward new self-similar solutions, which are very useful to completely reveal the essential behavior of the underlying physics. The targets are assumed to have a limited mass. The physical picture significantly contrasts with that well described by the orthodox self-similar solution for a semi-infinite planar rarefaction wave. The ion energy spectrum obtained by the model reproduces well experimental results obtained under different geometrical conditions. It is strictly shown that the hydrodynamic system of an accelerating foil admits a new self-similar solution describing the nonstationary ablation process, through which the payload mass decreases to burn out at the end. The system is appropriately solved as a novel eigenvalue problem such that the acceleration and the heat conductivity are restrictive with each other under the self-similar evolution.

Key words: laser-plasma acceleration of electrons and ions, two-fluid and multi-fluid plasmas, plasma sheaths, plasma simulation.
PACS numbers: 52.38.Kd, 52.30.Ex, 52.40.Kh, 52.65.-y.

1 Introduction

Dimensional and similarity theory provides one with the possibility of prior qualitative-theoretical analysis and the choice of a set for characteristic dimensionless parameters. The theory can be applied to the consideration of quite complicated phenomena and makes the processing of experiments much easier. What is more, at present, the competent setting and processing of experiments in inconceivable without taking into account dimensional and similarity reasoning. Sometimes at the initial stage of investigation of certain complicated phenomena, dimensional and similarity, theory is the only possible theoretical method, though the possibilities of this method should not be overestimated. The combination of similarity theory with considerations resulting from experiments or mathematical operations can sometimes lead to significant results. Most often dimensional and similarity theory is very useful for theoretical as well for practical use. All the results obtained with the help of this theory can be obtained quite easily and without much trouble.

A phenomenon is called self-similar if the spatial distributions of its properties at various moments of time can be obtained from one another by a similarity transformation. Establishing self-similarity has always represented progress for a researcher: self-similarity has simplified computations and the representation of the characteristics of phenomena under investigation. In handling experimental data, self-similarity has reduced what would seem to be a random cloud of empirical points so as to lie on a single curve of surface, constructed using self-similar variables chosen in some special way. Self-similarity enables us to reduce its partial differential equations to ordinary differential equations, which substantially simplifies the research. Therefore, with the help of self-similar solutions researchers have attempted to find the underlying physics. Self-similar solutions also serve as standards in evaluating approximate methods for solving more complicated problems.

Scaling laws, which are obtained as a result of the dimensional analysis and other methods, play an important role for understanding the underlying physics and applying them to practical systems. When constructing a full-scale system in engineering, numerical simulations will be first made in most cases. Its feasibility should be then demonstrated experimentally with a reduced-scale system. For astrophysical studies, for instance, such scaling considerations are indispensable and play a

decisive role in designing laboratory experiments. Then one should know how to design such a miniature system and how to judge whether two experimental results in different scales are hydrodynamically equivalent or similar to each other. Lie group analysis [1], which is employed in the present chapter, is not only a powerful method to seek self-similar solutions of partial differential equations (PDE) but also a unique and most adequate technique to extract the group invariance properties of such a PDE system. Lig group analysis and dimensional analysis are useful methods to find self-similar solutions in a complementary manner.

An instructive example of self-similarity is given by an idealized problem in the mathematical theory of linear heat conduction: Suppose that an infinitely stretched planar space ($-\infty < x < \infty$) is filled with a heat-conducting medium. At the initial instant $t = 0$ and at the origin of the coordinate $x = 0$, a finite amount of heat E is supplied instantaneously. Then the propagation of the temperature Θ is described by

$$\frac{\partial \Theta}{\partial t} = \kappa \frac{\partial^2 \Theta}{\partial x^2}, \tag{1}$$

where κ is the constant heat diffusivity of the medium. Then the temperature Θ at an arbitrary time t and distance from the origin x is given by

$$\Theta = \frac{E}{c\sqrt{4\pi\kappa t}} \exp\left(-\frac{x^2}{4\kappa t}\right), \tag{2}$$

where c is the specific heat of the medium. As a matter of fact, it is confirmed with the solution (2) that the integrated energy over the space is kept constant regardless of time:

$$\int_{-\infty}^{\infty} c\,\Theta(x,t)dx = E \tag{3}$$

The structure of Eq. (2) is instructive: There exist a temperature scale $\Theta_0(t)$ and a linear scale $x_0(t)$, both depending on time,

$$\Theta_0(t) = \frac{E}{c\sqrt{4\pi\kappa t}}, \quad x_0(t) = \sqrt{\kappa t}, \tag{4}$$

such that the spatial distribution of temperature, when expressed in these scales, ceases to depend on time at least in appearance:

$$\frac{\Theta}{\Theta_0} = f(\xi), \quad f(\xi) = \exp\left(-\frac{\xi^2}{4}\right), \quad \xi = \frac{x}{x_0}. \tag{5}$$

Suppose that we are faced with a more complex problem of mathematical physics in two independent variables x and t, requiring the solution of a system of partial differential equations on a variable $u(x,t)$ of the phenomenon under consideration. In this problem, self-similarity means the we can choose variable scales $u_0(t)$ and $x_0(t)$ such that in the new scales, $u(x,t)$ can be expressed by functions of one variable:

$$u = u_0(t)U(\xi), \quad \xi = x/x_0(t) \tag{6}$$

The solution of the problem thus reduces to the solution of a system of ordinary differential equations for the function $U(\xi)$.

At a certain point of analysis, dimensional consideration called Π-theorem plays a crucial role in a complementary manner to the self-similar method. Suppose we have some relationship defining a quantity a as a function of n parameters $a_1, a_2, \ldots, a_n$:

$$a = f(a_1, a_2, \ldots\ a_n). \tag{7}$$

If this relationship has some physical meaning, Eq. (7) must reflect the clear fact that although the numbers $a_1, a_2, \ldots, a_n$ express the values of corresponding quantities in a definite system of units of measurement, the physical law represented by this relation does not depend on the arbitrariness in the choice of units. To explain this, we shall divide the quantities $a, a_1, a_2, \ldots\ a_n$ into two groups. The first group, $a_1, \ \ldots\ a_k$, includes the governing quantities with independent dimensions (for example, length, mass, and time). The second group, $a, a_{k+1}, \ldots\ a_n$, contains quantities whose dimensions can be expressed in terms of dimensions of the quantities of the first group. Thus, for example, the quantity a has the dimensions of the product $a_1^p a_2^q \cdots a_k^r$, the quantity a_{k+1} has the dimensions of the

product $a_1^{p_{k+1}} a_2^{q_{k+1}} \cdots a_k^{r_{k+1}}$, etc. The exponents $p, q, \ldots$ are obtained by a simple arithmetic. Thus the quantities,

$$\Pi = \frac{a}{a_1^p a_2^q \cdots a_k^r},$$

$$\Pi_1 = \frac{a_{k+1}}{a_1^{p_{k+1}} a_2^{q_{k+1}} \cdots a_k^{r_{k+1}}}, \quad \ldots, \tag{8}$$

$$\Pi_{n-k} = \frac{a_n}{a_1^{p_n} a_2^{q_n} \cdots a_k^{r_n}},$$

turn out to be dimensionless, so that their values do not depend how one choose the units of measurement. This fact follows that the dimensionless quantities can be expressed in the form,

$$\Pi = \Phi(\Pi_1, \Pi_2, \ldots, \Pi_{n-k}), \tag{9}$$

where no dimensional quantity is contained. What should be stressed is that in the original relation (7), $n+1$ dimensional quantities $a, a_1, a_2, \ldots, a_n$ are connected, while in the reduced relation (9), $n-k+1$ dimensionless quantities Π, $\Pi_1, \Pi_2, \ldots, \Pi_{n-k}$ are connected with k quantities being reduced from the original relation.

We now apply dimensional analysis to the heat conduction problem considered above. Below we shall use the symbol [a] to give its dimension, as Maxwell first introduced, in terms of the unit symbols for length, mass, and time by the letters L, M, and T, respectively. For example, velocity v has its dimension $[v] = L/T$. Then the physical quantities describing the present system have following dimensions,

$$\begin{aligned} &[x] = L, \ [t] = T, \ [\kappa] = L^2 T^{-1}, \\ &[E] = ML^2 T^{-2}, \ [c\,\Theta] = ML^3 T^{-2}. \end{aligned} \tag{10}$$

From Eq. (10), in which five dimensional quantities $(n+1=5)$ under the three principal dimensions ($k=3$ for L, M, and T), one can construct the following dimensionless system with two dimensionless parameters Π and ξ $(=\Pi_1)$:

$$\Pi = f(\xi), \quad \Pi = \frac{c\,\Theta\sqrt{\kappa t}}{E}, \quad \xi = \frac{x}{\sqrt{\kappa t}}, \tag{11}$$

where f is unknown function. Substituting Eq. (11) for Eq. (1), one obtains,

$$f'' + \frac{1}{2}(f + \xi f') = 0, \tag{12}$$

where the prime denotes the derivative with respect to ξ; also the transform relation from partial to ordinary derivatives

$$\begin{aligned} \frac{\partial f(\xi)}{\partial t} &= -\frac{\xi}{2t} f'(\xi), \\ \frac{\partial f(\xi)}{\partial x} &= \frac{1}{\sqrt{\kappa t}} f'(\xi), \end{aligned} \tag{13}$$

are used. With the help of the boundary condition, $f'(0) = 0$, and Eq. (3), Eq. (12) is integrated to give

$$f(\xi) = \frac{1}{\sqrt{4\pi}} \exp\left(-\frac{\xi^2}{4}\right). \tag{14}$$

Thus Eqs. (11) and (14) reproduce the solution of the problem, Eq. (2).

What is described above is the simple and essential scenario of the approach in terms of self-similar solution and dimensional analysis, more details of which can be found, for example, in Refs. [1-4]. In the following subsections, we show three specific examples with new self-similar solutions, as reviews of previously published papers for readers' further understanding how to use the dimensional analysis and to find self-similar solutions: The first is on plasma expansion of a limited mass into vacuum, in which two fluids composed of cold ions and thermal electrons expands via electrostatic field [5]. The second is on laser-driven foil acceleration due to nonlinear heat conduction [6]. Finally, the third is an astrophysical problem, in which self-gravitation and non-linear radiation heat conduction determines the temporal evolution of star formation process in a self-organizing manner [7].

2 Isothermally expansion of laser-plasma with limited mass

Plasma expansion into a vacuum has been a subject of great interest for its role in basic physics and its many applications, in particular, its use in lasers. The applied laser parameter spans a wide range, $10^{10} \le \hat{I}_L \hat{\lambda}_L^2 \le 10^{19}$, where $\hat{I}_L$ is the laser

intensity normalized by $10^{11}\ W/cm^2$ and $\hat{\lambda}_L$ is the laser wavelength normalized by $1\ \mu m$ and. For $\hat{I}_L\hat{\lambda}_L^2 \geq 10^{14}$, generation of fast ions is governed by hot electrons with an increase in $\hat{I}_L\hat{\lambda}_L^2$. In this subsection, we focus on rather lower intensity range, $10^{10} \leq \hat{I}_L\hat{\lambda}_L^2 \leq 10^{14}$, where the effect of hot electrons is negligibly small and background cold electrons can be modeled by one temperature. Typical examples of applications for this range are laser driven inertial confinement fusion [8] and laser-produced plasma for an extreme ultra violet (EUV) light source [9]. As a matter of fact, the experimental data employed below for comparison with the analytical model were obtained for the EUV study. Theoretically, this topic had been studied only through hydrodynamic models until the early 1990s. In such theoretical studies, a simple planar (SP) self-similar solution has often been used [10]. In the SP model, a semi-infinitely stretched planar plasma is considered, which is initially at rest with unperturbed density ρ_0. At $t = 0$, a rarefaction wave is launched at the edge to penetrate at a constant sound speed c_s into the unperturbed uniform plasma by being accompanied with an isothermal expansion. The density and velocity profiles of the expansion are given by [11] $\rho = \rho_0 \exp[-(1 + x/(c_s t)]$ and $v = c_s + x/t$, respectively. The solution is indeed quite useful when using relatively short laser pulses or thick targets such that the density scale can be kept constant throughout the process.

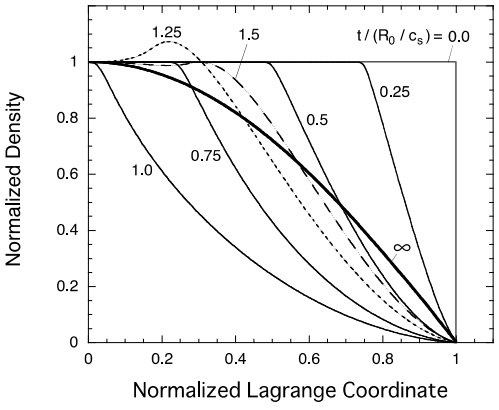

Figure 1 – Temporal evolution of the density profile of a spherical isothermal plasma, which is normalized by that at the center; R_0 and c_s are the initial radius and the sound speed, respectively. After the rarefaction wave reflects at the center, the density distribution asymptotically approaches its final self-similar profile (the thick curve with "∞").

However, in actual laser-driven plasmas, a shock wave first penetrates the unperturbed target instead of the rarefaction wave. Once this shock wave reaches the rear surface of a finite-sized target and the returning rarefaction wave collides with the penetrating rarefaction wave, the entire region of the target begins to expand, and thus the target disintegration sets in. If the target continues to be irradiated by the laser even after the onset of target disintegration, the plasma expansion and the resultant ion energy spectrum are expected to substantially deviate from the physical picture given by the SP solution. Figure 1 demonstrates a simplified version of the physical picture mentioned above with temporal evolution of the density profile obtained by hydrodynamic simulation for an isothermal expansion. A spherical target with density and temperature profiles being uniform is employed as an example. In Figure 1, the density is always normalized by one at the center, and the labels assigned to each curve denote the normalized time $t/(R_0 c_s)$, where R_0 is the initial radius. The horizontal Lagrange coordinate is normalized to unity at the plasma edge. It can be discerned from Figure 1 that the profile rapidly develops in the early stage for $t/(R_0 c_s) \leq 1$. After the rarefaction wave reflects at the center, the density distribution asymptotically approaches its final self-similar profile (the thick curve with label "∞"), which is expressed in the Gaussian form, $\rho \propto \exp[-(r/R)^2]$ as will be derived below. The initial and boundary conditions employed in Figure 1 are substantially simplified such that the laser-produced shock propagation and resultant interactions with the rarefaction wave are not described. However, the propagation speeds of the shock and rarefaction waves are always in the same order as the sound speed c_s of the isothermally expanding plasma. Therefore the physical picture shown in Figure 1 is expected to be qualitatively valid also for realistic cases. Below, we present a self-similar solution for the isothermal expansion of limited masses [5]. The solution explains plasma expansions under relatively long laser pulses or small-sized targets so that the solution responds to the above argument on target disintegration. Note that other self-similar solutions of isothermal plasma expansion have been found for laser-driven two-fluid expansions in light of ion acceleration physics [9] and heavy-ion-driven cylindrical x-ray converter [12], though they are not discussed here.

2.1. Isothermal expansion

The plasma is assumed to be composed of cold ions and electrons described by one temperature T_e, which is measured in units of energy as follows. Furthermore, the electrons are assumed to obey the Boltzmann statistics,

$$n_e = n_{ec} \exp(e\Phi/T_e)\,, \tag{15}$$

where $n_{ec}(t)$ is the temporal electron density at the target center, e is the elementary charge, and $\Phi(r,t)$ is the electrostatic potential, the zero-point of which is set at the target center, i.e., $\Phi(0,t) = 0$. The potential Φ satisfies the Poisson equation,

$$\frac{1}{r^{\alpha-1}}\frac{\partial}{\partial r}\left(r^{\alpha-1}\frac{\partial \Phi}{\partial r}\right) = 4\pi e(n_e - Zn_i)\,, \tag{16}$$

where Z is the ionization state; the superscript α stands for the applied geometry such that α = 1, 2, and 3 correspond to planar, cylinder, and spherical geometry, respectively. Throughout the present analysis, the electron temperature T_e and the ionization state Z are assumed to be constant in space and time.

An ion in the plasma is accelerated via the electrostatic potential in the form,

$$\frac{\partial v}{\partial t} + v\frac{\partial v}{\partial r} = -\frac{Ze}{m_i}\frac{\partial \Phi}{\partial r}\,, \tag{17}$$

where m_i is the ion mass and v is the ion velocity. Note that, in the following, we consider such a system that the plasma has quasi-neutrality, i.e., $n_e \approx Zn_i$, where n_i and n_e are the number densities of the ions and the electrons, respectively. Equations (15) and (17) are combined to derive a single-fluid description,

$$\frac{\partial v}{\partial t} + v\frac{\partial v}{\partial r} = -\frac{c_s^2}{\rho}\frac{\partial \rho}{\partial r}\,, \tag{18}$$

where $c_s = \sqrt{ZT_e/m_i}$ is the sound speed. Also, a fluid element with mass density $\rho(r,t) = m_i n_i$ satisfies the following mass conservation law,

$$\frac{\partial \rho}{\partial t} + \frac{1}{r^{\alpha-1}}\frac{\partial}{\partial r}(r^{\alpha-1}\rho v) = 0\,. \tag{19}$$

We now seek a self-similar solution to Eqs. (18) and (19) on $\rho(r,t)$ and $v(r,t)$ under the similarity ansatz,

$$v = \dot{R}\xi\,,\ \ \xi \equiv \frac{r}{R}\,, \tag{20}$$

$$\rho = \rho_{00}\left(\frac{R}{R_0}\right)^{-\alpha} G(\xi), \tag{21}$$

where $R(t)$ stands for a time-dependent characteristic system size, and ξ is the dimensionless similarity coordinate; the over-dot in Eq. (20) denotes the derivative with respect to time; $\rho_{00} \equiv \rho(0,0)$ and $R_0 \equiv R(0)$ are the initial central density and the size, respectively; $G(\xi)$ is a positive unknown function with the normalized boundary condition $G(0) = 1$. Then, Eqs. (15) and (21) give

$$n_e \approx n_{ec}(t)G(\xi) \approx Z\frac{\rho_{00}}{m_i}\left(\frac{R}{R_0}\right)^{-\alpha} G(\xi), \tag{22}$$

Under the similarity ansatz, Eqs. (20) and (21), the mass conservation, Eq. (19), is automatically satisfied. Substituting Eqs. (20) and (21) for Eq. (18), and making use of the derivative rules, $\partial/\partial r = R^{-1}(d/d\xi)$ and $\partial/\partial t = -\xi\dot{R}R^{-1}(d/d\xi)$, one obtains the following ordinary differential equations in the form of variable separation,

$$\frac{R\ddot{R}}{c_s^2} = -\frac{G'}{\xi G} = \psi_0\,, \tag{23}$$

where $\psi_0(>0)$ is a separation constant, and the prime denotes the derivative with respect to ξ. Without losing generality, the constant ψ_0 can be set equal to an arbitrary numerical value, because this is always possible with a proper normalization of R and ξ. Here, just for simplicity, we set $\psi_0 = 2$ in Eq. (23). Then the spatial profile of the density, $G(\xi)$, is straightforwardly obtained under $G(0) = 1$ in the form [13-14],

$$G(\xi) = \exp(-\xi^2)\,. \tag{24}$$

As was seen in Figure 1, the density profile of isothermally expanding plasma with a limited mass is found to approach asymptotically the solution, Eq. (24), even if it has a different profile in the beginning. Meanwhile, $R(t)$ in Eq. (23) cannot be given explicitly as a function of time but has the following integrated forms,

$$\dot{R} = 2c_s\sqrt{\ln(R/R_0)}\,, \tag{25}$$

$$\frac{c_s t}{R_0} = \frac{1}{2}\int_1^{RR_0} \frac{dx}{\sqrt{\ln x}}\,, \tag{26}$$

where in obtaining Eqs. (25) and (26), the system is assumed to be initially at rest, i.e., $\dot{R}(0) = 0$. Here it should be noted that Eqs. (23) - (26) do not explicitly include the geometrical index α, and therefore they apply to any geometry.

Based on the solution given above, some other important quantities are derived as follows. First, the total mass of the system M_0 is conserved and given with the help of Eqs. (21) and (24) in the form,

$$M_0 == (4\pi)_\alpha \rho_{00} R_0^\alpha \int_0^\infty \xi^{\alpha-1} \times \\ \times \exp(-\xi^2)\, d\xi = \left(\sqrt{\pi}R_0\right)^\alpha \rho_{00}\,, \tag{27}$$

with

$$(4\pi)_\alpha \equiv \begin{cases} 2, & (\alpha = 1) \\ 2\pi, & (\alpha = 2) \\ 4\pi, & (\alpha = 3) \end{cases} = \frac{2\pi^{\alpha/2}}{\Gamma(\alpha/2)}\,, \tag{28}$$

where Γ is the Gamma function. Although the quantitative meaning of $R(t)$ was somewhat unclear when first introduced in Eq. (20), it can be now clearly understood by relating it to the temporal central density, $\rho_c(t) \equiv \rho(0,t) \approx m_i n_{ec}(t)/Z$, with the help of Eqs. (21) and (27) in the form,

$$R(t) = \frac{1}{\sqrt{\pi}}\left(\frac{M_0}{\rho_c(t)}\right)^{1/\alpha}. \tag{29}$$

Additionally the potential Φ and corresponding electrostatic field $E = -\nabla\Phi$ are obtained from Eqs. (15), (21), (22), and (24) in the following forms,

$$\frac{e\Phi}{T_e} = -\xi^2\,, \tag{30}$$

$$\frac{eE}{T_e} = \frac{2\xi}{R}\,. \tag{31}$$

The above field quantities contrast well with the fields of the SP solution obtained for a semi-infinitely stretched planar plasma: $e\Phi/T_e = -1 - x/c_s t$ and $eE/T_e = 1/c_s t$ for $x/c_s t \geq -1$ and $t > 0$. It is here worth emphasizing that the electrostatic field increases linearly with ξ for the present model, while it is constant in space for the SP model. Furthermore, the kinetic energy of the system $E_k(t)$ is given with the help of Eqs. (20), (21) and (27) by

$$E_k = \frac{(4\pi)_\alpha}{2}\rho_{00}R_0^\alpha \dot{R}^2 \int_0^\infty \xi^{\alpha+1} \times \\ \times \exp(-\xi^2)\, d\xi = \frac{\alpha}{4} M_0 \dot{R}^2, \tag{32}$$

while the internal (thermal) energy of the system $E_i(t)$ is kept constant,

$$E_i = \frac{3M_0 Z T_e}{2m_i} = \frac{3}{2} M_0 c_s^2\,. \tag{33}$$

Correspondingly, the power required to keep the isothermal expansion, $P(t) = dE_k/dt$, is given from Eqs. (23), (25), and (32) in the form,

$$P/P_0 = \sqrt{\ln(R/R_0)}\,/(R/R_0\,), \tag{34}$$

where $P_0 = 2\alpha M_0 c_s^3/R_0$.

The ion energy spectrum is a physical quantity of high interest. In the present model, the kinetic energy of an ion in flight directly relates its location, in other words, the further an ion is located, the faster it flies. Then, the number of ions contained in an infinitesimally narrow area of the similarity coordinate between ξ and $\xi + d\xi$ is given by

$$dN = (4\pi)_\alpha n_{i00} R_0^\alpha \xi^{\alpha-1} \exp(-\xi^2)\, d\xi\,, \tag{35}$$

where $n_{i00} = \rho_{00}/m_i$ is the initial number density of the ions at the center. Meanwhile, the kinetic energy of an ion at ξ is $\varepsilon = m_i \dot{R}^2 \xi^2/2$, and therefore

$$d\varepsilon = m_i \dot{R}^2 \xi d\xi\,. \tag{36}$$

From Eqs. (35) and (36), the ion energy spectrum is obtained,

$$\frac{d\hat{N}}{d\hat{\varepsilon}} = \frac{\hat{\varepsilon}^{(\alpha-2)/2}\exp(-\hat{\varepsilon})}{\Gamma(\alpha/2)}, \tag{37}$$

where $\hat{N} \equiv N/N_0$ and $\hat{\varepsilon} \equiv \varepsilon/\varepsilon_0$ are normalized quantities with

$$\varepsilon_0(t) = m_i\dot{R}^2/2\,, \tag{38}$$

$$N_0 = (\sqrt{\pi}R_0)^{\alpha} n_{i00}\,. \tag{39}$$

It should be noted that, for α = 3, the energy spectrum, Eq. (37), coincides with the well-known Maxwellian energy distribution; this is not just a coincidence because an isotropically heated mass always has such a distribution.

Although the spectrum, Eq. (37), is for the ion number density, another spectrum for the energy density, $dE_k/d\varepsilon$, is an even more interesting quantity. It can be easily obtained quite in the same manner as for $dN/d\varepsilon$ taking the specific kinetic energy $v^2/2$ into account:

$$\frac{dE_k}{d\hat{\varepsilon}} = \frac{\varepsilon_0 N_0}{\Gamma(\alpha/2)}\hat{\varepsilon}^{\alpha/2}\exp(-\hat{\varepsilon})\,. \tag{40}$$

The peak value of Eq. (40) is attained at $\hat{\varepsilon} = \alpha/2$, which is three times higher than that of Eq. (37) for the spherical case ($\alpha = 3$).

2.2. Comparison with experiments

We apply the analytical model to two different laser experiments focusing on the ion energy spectrum. The two experimental results were separately obtained under different conditions by means of the time-of-flight method. In both cases, the laser conditions were almost the same, i.e., the wavelength $\lambda_L = 1.06\,\mu m$, the irradiation intensity $I_L = 0.5 - 1.0 \times 10^{11}\,W/cm^2$, and the pulse length $\tau_L \sim 10\,ns$ with a sufficiently large F-number of a focal lens. Moreover, the target thicknesses were $R_0 \sim 10\,\mu m$. Once the key laser parameters, I_L and τ_L, are given, the other basic parameters required for the model analysis are calculated. For example, the plasma temperature is roughly estimated from the power balance, $\eta_a I_L \approx 4\rho_{cr}c_s^3$ [15], where η_a is the absorption efficiency and ρ_{cr} is the critical mass density:

$$T_e\,[eV] = 27(A/Z)^{1/3}\hat{\lambda}_L^{4/3}\left(\eta_a \hat{I}_L\right)^{2/3}, \tag{41}$$

where A is the ion mass number. The corresponding sound speed turns out to be in the order of $10^6 cm/s$, and the disintegration time $\sim 2R_0/c_s$ (recall Figure 1) is calculated to be about 1 ns ($\ll \tau_L \sim 10\,ns$). The normalized radius R/R_0 at the laser turn-off is obtained by Eq. (26) as a function of the normalized time $\tau_L/(R_0/c_s)$. In addition, the scale length of the plasma expansion is $c_s\tau_L \sim 100\,\mu m (\gg R_0 \sim 10\,\mu m)$. Therefore, the present self-similar analysis is considered to be applicable to the experiments under consideration. From the above key numerical values, the characteristic ion kinetic energy at the laser turn-off defined by Eq. (38) is roughly estimated to be $\varepsilon_0 = 2.5 - 3.5$ keV.

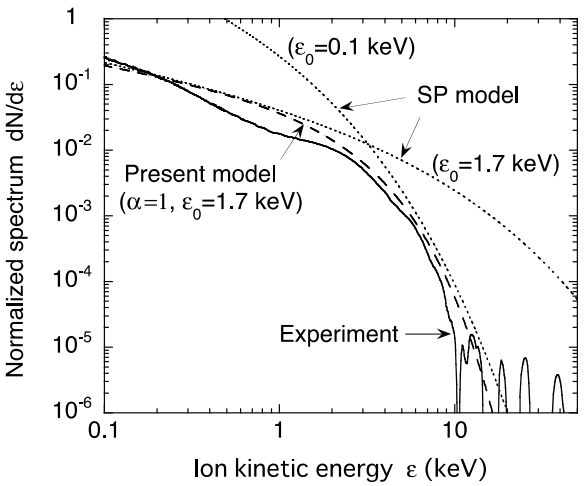

Figure 2 – Comparison of the experimental result (solid line) and the analytical curve (dashed line) obtained by Eq. (37) under planar geometry. Dotted curves for reference are obtained by the SP model, Eq. (42)

In the first case, a laser beam was irradiated on a spherical target with diameter of $500\,\mu m$, which was composed of $8\mu m$-thick plastic shell coated by a 100 nm-thick tin (Sn) layer. In this case, the plasma expansion during the laser irradiation can be regarded as quasi-planar, because the plasma scale ~$100\,\mu m$ is appreciably smaller than the laser spot size $\sim 500\,\mu m$. As mentioned in the introduction, the purpose of the Sn-coat was to observe the characteristics of the EUV light and energetic ion fluxes emitted from the Sn plasma. The detector was tuned to observe massive Sn ions in the direction of 30 degrees with respect to the beam axis. Figure 2 shows the ion energy spectrum comparing the experimental result (solid line) and the analytical curve (dashed line) obtained by Eq. (37) with a fitted numerical factor $\varepsilon_0 = 1.7$ keV and $\alpha = 1$ (planar

geometry). With respect to the vertical axis, the physical quantities are properly normalized such that the peak values stay in the order of unity. The fluctuated structure of the experimental data for $\varepsilon > 10$ keV cannot be clearly judged as concerns whether the signals simply span the region with less precision of diagnosis, or whether they should be attributed to other causes such as carbon ions, protons, and photons. In Figure 2, two other curves (dotted lines) are also plotted for comparison. They are obtained by the SP model [16],

$$\frac{dN}{d\hat{\varepsilon}} \propto \frac{\exp\left(-\sqrt{\hat{\varepsilon}}\right)}{\sqrt{\hat{\varepsilon}}}, \tag{42}$$

where $\varepsilon_0 = 1.7$ keV and $\varepsilon_0 = 0.1$ keV are used to draw the fitted curves to relatively low and high energy regions, respectively. It can be seen that it is hard to reproduce the experimental result by Eq. (42). The essential difference of the two analytical models is attributed to their density profiles, i.e., $\rho \propto \exp(-\xi^2)$ for the present model and $\rho \propto \exp(-\xi)$ for the SP model. This can be elaborated on as follows: The pressure scale decreases with time all over the region in the present model, while it is kept constant in time in the SP model. Therefore, the ions in the former model are less accelerated due to the pdV work than those in the latter model.

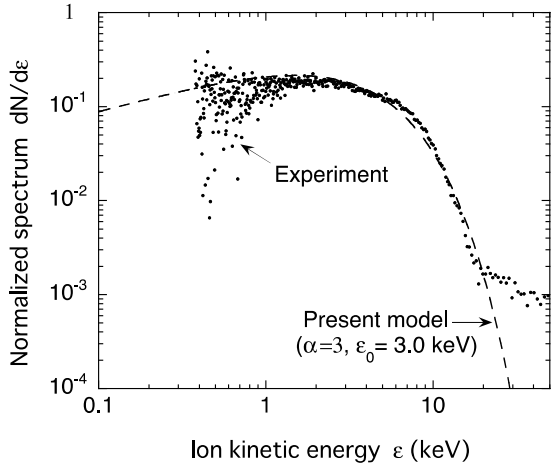

Figure 3 – Comparison of the experimental result (dots) and the analytical curve (dashed line) obtained by Eq. (37) under spherical geometry

In the second case, a laser beam was irradiated from a single side with a liquid-Xe jet ejected through a nozzle with diameter of 30 μm. The focal spot size was also 30 μm in diameter. Therefore, the resultant plasma expansion was very likely unsymmetrical. In this case, however, the specific mass can expand into much larger space three-dimensionally than in the first case, and thus is regarded as a quasi-spherical expansion ($\alpha = 3$). Figure 3 shows the experimental result and an analytical curve obtained by Eq. (37) with a fitted numerical factor $\varepsilon_0 = 3.0$ keV. Again, with respect to the vertical axis, the physical quantities are properly normalized such that the peak values stay in the order of unity. The ion fluxes were observed at an angle of 45 degrees with respect to the laser beam axis. The experimental signals strongly fluctuate at energies close to the lowest detection limit at around $\varepsilon \sim 400$ eV, but are otherwise well reproduced by the analytical curve.

3. Laser-driven nonstationary accelerating foil due to nonlinear heat conduction

When one side of a thin planar foil is heated by an external heat source, typically by laser or thermal x-ray radiation, the heated material quickly expands into vacuum with its density being reduced drastically - this phenomenon is called “ablation”. In inertial confinement fusion (ICF) research, for example, it is indispensable to correctly understand the shell acceleration due to ablation. Thereby self-similar solutions play a crucial role in the analysis and prediction of the detailed behavior of the shell acceleration. Although some analytical models have been proposed to study the shell acceleration due to mass ablation [17-19], most of them have assumed a stationary ablation layer. In Ref. [20], for example, reported a self-similar solution for the ablative heat wave. In the solution, however, the ablation surface is ideally treated such that the density goes to infinity, and the surface does not accelerate. Below, we present a new self-similar solution [6], which describes non-stationary acceleration dynamics of a planar foil target ablatively driven by non-linear heat transfer. The most striking differences from the other models are that the target has a decreasing mass with a peak density, and that it has a distinct shell/vacuum boundary, where the density and the temperature converge to null.

3.1. Basic equations and similarity ansatz

Suppose that a planar shell is being accelerated in the positive direction of the x-axis in an inertial laboratory frame via the recoil force due to the ablation. The characteristic scale length of the shell $D(t)$ decreases with time. Let us assume that the shell is burnt out at the origin of the coordinates, i.e., $D(0) = 0$ at $x = 0$. One can always find such an

inertial frame by appropriately choosing relative position and velocity to another reference inertial frame. In this case the shell velocity is initially ($t < 0$) negative, its absolute value gradually decreases due to the positive acceleration, and finally the burned-out shell halts at $(x,t) = (0,0)$. The fluid system is then described by the following equations:

$$\frac{\partial \rho}{\partial t} + \frac{\partial (\rho v)}{\partial x} = 0\,, \tag{43}$$

$$\frac{\partial v}{\partial t} + v\frac{\partial v}{\partial x} = -\frac{\partial p}{\partial x}, \tag{44}$$

$$\rho\left(\frac{\partial \epsilon}{\partial t} + v\frac{\partial \epsilon}{\partial x}\right) + p\frac{\partial v}{\partial x} = \frac{\partial}{\partial x}\left(\kappa\frac{\partial T}{\partial x}\right), \tag{45}$$

where ρ is the mass density, v is the flow velocity, ϵ is the specific internal energy, T is the temperature in units of energy, and κ is the thermal conductivity. We assume an ideal gas equation of state in the form,

$$p = \rho T,\ \epsilon = T/(\gamma - 1), \tag{46}$$

where γ is the specific heats ratio. We assume that the thermal conductivity is expressed in the following power-law form with m, n, and κ_0 being constants,

$$\kappa = \kappa_0 T^n/\rho^m. \tag{47}$$

We introduce the following well-known similarity ansatz [21] to eliminate the temporal dependence of the system and thus to find a self-similar solution:

$$\eta = x/D(t)\,,\ D(t) = A(-t)^\alpha\,,\ \alpha \geq 1\,, \tag{48}$$

$$v = \alpha A(-t)^{\alpha-1}u(\eta)\,, \tag{49}$$

$$T = (\alpha A)^2(-t)^{2(\alpha-1)}\theta(\eta)\,, \tag{50}$$

$$\rho = B(-t)^\beta g(\eta)\,,$$
$$\beta = \frac{2(n-1)(\alpha-1)-1}{1+m}, \tag{51}$$

where η is the self-similar variable; $u(\eta)$, $\theta(\eta)$, and $g(\eta)$ stand for the self-similar profiles of the velocity, temperature, and density, respectively; α, A and B are arbitrary constants. In most of numerical calculations in this paper, we employ $\alpha = 2$ (constant acceleration), $(m,n) = (0,5/2)$ (electron heat conductivity) and $\gamma = 5/3$ as a reference case. The constraint, $\alpha \geq 1$, in Eq. (48) stems from Eqs. (49) and (50) in order that v and T do not diverge to infinity as $t \to 0$. The limiting value, $\alpha = 1$, corresponds to a special case, where the characteristic scale of v and T are kept constant in time, while $\alpha = (2n-1)/2(n-1) = 4/3$ corresponds to another special case, where the density scale does not change in time, i.e., $\beta = 0$ [see Eq. (51)].

Using ansatz (48) - (51), Eqs. (43) - (45) are reduced to the following set of ordinary differential equations:

$$(u+\eta)g' + \left(u' - \frac{\beta}{\alpha}\right)g = 0\,, \tag{52}$$

$$(u+\eta)\,u' + (\alpha^{-1}-1)u + (g\theta)'/g = 0\,, \tag{53}$$

$$(\gamma-1)^{-1}[(u+\eta)\theta' + 2(\alpha^{-1}-1)\theta] + \\ +\theta u' = Kg^{-1}(g^{-m}\theta^n\theta')' \tag{54}$$

where the prime denotes the derivative with respect to η, and

$$K = \kappa_0\alpha^{2n-1}A^{2n-2}B^{-1-m} \tag{55}$$

is a dimensionless parameter. Solving Eqs. (52) and (53) algebraically for g' and u', one finds that a singular point appears when $u + \eta = \pm\sqrt{\theta}$ (more details on the singular point will be given later). Let η_s, u_s, g_s, and θ_s be their values at the singular point. Here we introduce re-normalized variables, ξ, U(ξ), G(ξ), and Θ(ξ):

$$\xi = \frac{\eta - \eta_s}{\sqrt{\theta_s}}\,, \qquad \xi = \frac{u - \eta_s}{\sqrt{\theta_s}}\,,$$
$$G = \frac{g}{g_s}\,, \qquad \Theta = \frac{\theta}{\theta_s}, \tag{56}$$

At the singular point, $\xi = 0$, the re-normalized variables are specified to be

$$U(0) = -1, \quad G(0) = 1, \quad \Theta(0) = 1, \tag{57}$$

where we employ the flow direction such that $u_s + \eta_s = -\sqrt{\theta_s}$. Equations (10) - (12) are then transformed to

$$(U+\xi)\,G' + (U' - \beta/\alpha)G = 0\,, \tag{58}$$

$$(U+\xi)U' + (\alpha^{-1}-1)U + \\ +(G\Theta)'/G + K_1 = 0\,, \tag{59}$$

$$(\gamma-1)^{-1}[(U+\xi)\Theta' + 2(\alpha^{-1}-1)\Theta] + \\ +\Theta U' = K_2 G^{-1}(G^{-m}\Theta^n\Theta')' \tag{60}$$

where the prime hereafter denotes the derivative with respect to ξ, and

$$K_1 = (1-\alpha^{-1})\eta_s/\sqrt{\theta_s}\,, \\ K_2 = K\theta_s^{n-1}g_s^{-m-1}\,, \tag{61}$$

are dimensionless constants representing the gravity (acceleration) and the heat conductivity, respectively. Thus the system is clearly defined by Eqs. (57) - (60). Equations (58) and (59) yield

$$G' = \frac{\Delta_2}{\Delta_1}G\,, \\ U' = \frac{\beta}{\alpha} - (U+\xi)\frac{\Delta_2}{\Delta_1}, \tag{62}$$

where

$$\Delta_1 = (U+\xi)^2 - \Theta\,, \tag{63}$$

$$\Delta_2 = \left(\frac{\beta}{\alpha}\right)(U+\xi) + \\ +(\alpha^{-1}-1)U + \Theta' + K_1\,. \tag{64}$$

It is clear that G′ and U′ in Eq. (62) are singular when $\Delta_1 = 0$. This singular point corresponds to the sonic point, where the flow velocity relative to the surface $\xi = const$ is equal to the local isothermal sound speed. An integrated curve which is physically acceptable is expected to pass this singular sonic point smoothly, the condition of which is given by

$$\Delta_1 = \Delta_2 = 0\,. \tag{65}$$

Since $\xi = 0$ is the singular point, one should start numerical integration at its infinitesimally adjacent point. One then needs the four derivatives $G'(0)$, $U'(0)$, $\Theta'(0)$, and $\Theta''(0)$, which are fully provided by relation (65). At $\xi = 0$, the derivatives of Eq. (62) are reduced from L'Hopital's theorem to

$$G' = \frac{\Delta_2'}{\Delta_1'}\,, \quad U' = \frac{\beta}{\alpha} + \frac{\Delta_2'}{\Delta_1'}\,. \tag{66}$$

Thus all the four derivatives at the sonic point are explicitly obtained from Eqs. (57) - (60), and (66).

The present system has another singular point at the vacuum interface, the coordinate at which, $\xi = \xi_v$, is an eigenvalue of the system. On the vacuum interface the relative flow velocity to the free surface vanishes, i.e., $U(\xi_v) + \xi_v = 0$, which can also be interpreted as the definition of the free surface. Moreover at $\xi = \xi_v$ the pressure and thus the density are expected to vanish coherently, because practically no heat conduction prevails in this front region (typically characterized such that $G \gg 1$, $\Theta \ll 1$, and $(U+\xi)^2 \ll \Theta$) and thus the specific entropy is kept constant in time. It is then shown that Eqs. (16) and (18) (neglecting the heat conduction) have the adiabatic integral with an arbitrary constant c_0 [4]:

$$\Theta(U+\xi)^\mu G^{\mu+1-\gamma} = c_0, \\ \mu \equiv \frac{2(1-\alpha)+\beta(\gamma-1)}{\alpha+\beta}. \tag{67}$$

The vacuum interface is a singular point of the adiabatic flow of the saddle type [22], where the spatial profiles in the vicinity of $\xi = \xi_v$ is worked out from Eqs. (58) - (60) to a first-order approximation in $(\xi_v - \xi)$:

$$\Theta \approx \frac{\big((\gamma+1)\alpha-2\big)(\alpha K_1 + (\alpha-1)\xi_v)}{(\alpha+\beta)\gamma} \times \\ \times (\xi_v - \xi), \tag{68}$$

$$U + \xi \approx -\frac{\gamma+1-2\alpha^{-1}}{\gamma}(\xi_v - \xi), \tag{69}$$

$$G \approx c_1(\xi_v - \xi)^\nu, \quad \nu \equiv \frac{-\alpha+\beta\gamma+2}{\alpha(\gamma+1)-2}, \tag{70}$$

where c_1 is an arbitrary constant; $c_1 \approx G_a(\xi_v - \xi_a)^{-\nu}$ for a relatively high aspect shell, i.e., $G_a/(\xi_v - \xi_a) \gg 1$, where G_a and ξ_a are their corresponding values at the density peak; G_a and ξ_a are also eigenvalues of the system as will be given below together with ξ_v. In particular, under constant acceleration ($\alpha = 2$), the velocity becomes constant, $U = -\xi_v$, and $G \propto (\xi_v - \xi_a)$ apart from a linear temperature profile in space, as one can predict from Eqs. (69) and (70).

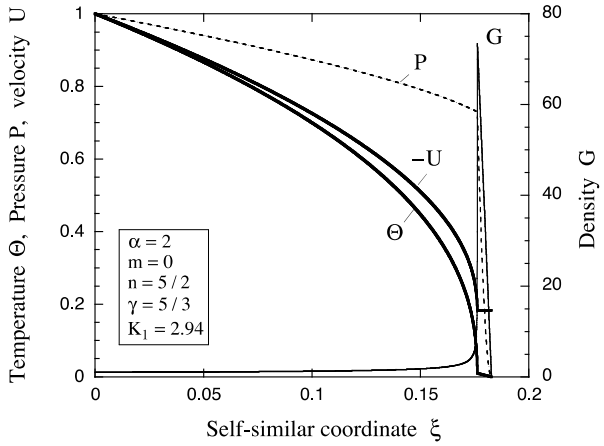

Figure 4 – Eigenstructure of the accelerated shell under a constant gravity ($\alpha = 2$)

3.2. Two dimensional eigenvalue problem and numerical results

Although one can start the numerical integration at $\xi = 0$ toward the positive direction of ξ-axis, it soon turns out that such numerical integrations produce physically unacceptable pictures under an arbitrary set of the values of K_1 and K_2 such that $G \to \infty$ on its way in the integration without showing the converging behavior, Eqs. (68) - (70), at the vacuum boundary. Therefore the present system is supposed to be an eigenvalue problem, in which only some special combinations of K_1 and K_2 can produce the converging behavior expected as a physically meaningful solution [7].

Figure 4 shows such an eigenstructure numerically obtained for the density G, the temperature Θ, the velocity U, and the pressure $P = G\Theta$ under the fixed parameters given in Figure 4. As mentioned earlier, the spatial profiles thus obtained strikingly contrast with ones for the stationary ablation models [16, 17].

Figure 5 shows the magnified view around the ablation surface of Figure 4, in which the mass flux relative to the surface with $\xi = const$, $F \equiv -(U + \xi)G$, is additionally depicted. Surprisingly the predicted profiles, (68) - (70), apply not only to the vicinity of the vacuum boundary but also to almost all the region beyond the ablation surface ($\xi > 0.1763$). This in turn supports the earlier argument that the heat conduction in the shell is practically negligible. It should also be noted that at $\xi = \xi_a$ the physical quantities seemingly have a sharp jump in their derivatives. However, all those quantities change smoothly but on a very narrow range, which can be observed in the further magnified view for G in the upper right corner in Figure 5. The characteristic scale length of the drastic change in the physical quantities can be roughly estimated from Eq. (60) to be $\Delta\xi_a \sim \Theta_a^n/|U_a|\, G_a^{1+m} \sim \mathcal{O}(10^{-5})$ as can be observed in Figure 5.

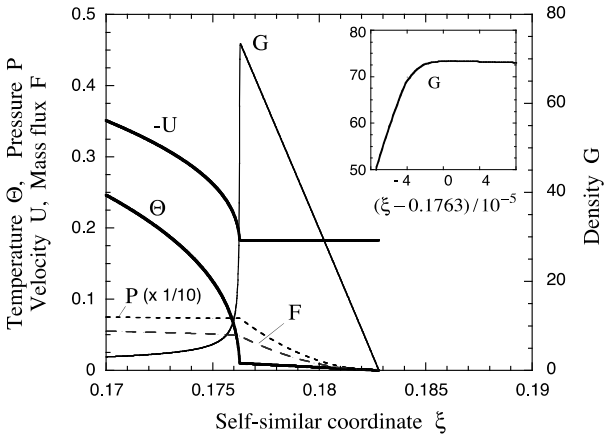

Figure 5 – Magnified view of Figure 4 around the ablation surface

4. Conclusions

The crucial role of dimensional analysis and self-similarity are discussed in the introduction and the three subsequent examples. Self-similar solutions for individual cases have been demonstrated to be derivable by applying the Lie group analysis to the set of PDE for the hydrodynamic system, taking nonlinear heat conductivity into account as the decisive physical ingredient. The scaling laws for thermally conductive fluids are conspicuously different from those for adiabatic fluids (not discussed in the present chapter; see Ref. [8] for details. The former has one freedom less than the latter due to the additional constraint of thermal conductivity. If a thermo-hydrodynamic system comprises multiple heat conduction mechanisms, self-similarity cannot be expected in a vigorous sense except for special cases. However, self-similarity and scaling laws can always be found at least in an approximate manner, by shedding light on the dominant conduction mechanism, which should give the basis of system design and diagnostics for scaled experiments for individual cases. The necessity of dimensional analysis and finding self-similar solutions is encountered in many problems over wide ranges of research. The simple general scheme and the examples mentioned in this chapter will help the reader who encounters a similar situation in his or her investigation find the underlying physics and prepare further theoretical and experimental setup.

References

1. S. Lie. Theorie der Transformationsgruppen. – New York: Chelsea, 1970. – 2043 p.
2. G.I. Barenblatt. Similarity, self-similarity, and intermediate asymptotics. – New York: Consultants Bureau, 1979. – 218 p.
3. L.I. Sedov. Similarity and dimensional methods in mechanics. – New York: Academic, 1959. – 380 p.
4. Ya.B. Zel'dovich, Yu.P. Raizer. Physics of shock waves and high temperature hydrodynamic phenomena. – New York: Academic Press, 1966. – 464 p.
5. M. Murakami, Y.-G. Kang, K. Nishihara, S. Fujioka, H. Nishimura. Ion energy spectrum of expanding laser-plasma with limited mass // Phys. Plasmas – 2005. – Vol. 12. – P. 062706.
6. M. Murakami, T. Sakaiya, J. Sanz. Self-similar ablative flow of nonstationary accelerating foil due to nonlinear heat conduction // Phys. Plasmas – 2007. – Vol. 14. – P. 022707.
7. M. Murakami, K. Nishihara, T. Hanawa. Self-similar gravitational collapse of radioactively cooling spheres // Astrophysical Journal – 2004. – Vol. 607. – P. 879.
8. M. Murakami, Sh. Iida. Scaling laws for hydrodynamically similar implosions with heat conduction // Phys. Plasmas – 2002. – Vol. 9. – P. 2745.
9. M. Murakami, M. M. Basko. Self-similar expansion of finite-size non-quasi-neutral plasmas into vacuum: Relation to the problem of ion acceleration // Phys. Plasmas – 2006. – Vol. 13. – P. 012105.
10. A.V. Gurevich, L.V. Pariiskaya, L.P. Pitaevskii. Self-similar motion of rarefied plasma // Sov. Phys. JETP – 1966. – Vol. 22. – P. 449.
11. L.D. Landau, E.M. Lifshitz. Fluid Mechanics. – New York: Pergamon, 1959. – 551 p.
12. M. Murakami, J. Meyer-Ter-Vehn, R. Ramis. Thermal x-ray emission from ion-beam-heated matter // J. X-ray Sci. Technol. – 1990. – Vol. 2. – P. 127.
13. M. A. True, J. R. Albritton, E. A. Williams. Fast ion production by suprathermal electrons in laser fusion plasmas // The Physics of Fluids – 1981. – Vol. 24. – P. 1885;
14. R. A. London, M. D. Rosen. Hydrodynamics of exploding foil x-ray lasers // Phys Fluids – 1986. – Vol. 29. – P. 3813-3822.
15. M. Murakami, J. Meyer-ter-Vehn. Indirectly driven targets for inertial confinement fusion // Nucl. Fusion – 1991. – Vol. 31. – P. 1315.
16. P. Mora. Plasma Expansion into a vacuum // Phys. Rev. Lett. – 2003. – Vol. 90. – P. 185002.
17. S. J. Gitomer, R.L. Morse, B.S. Newberger. Structure and scaling laws of laser□driven ablative implosions // Phys. Fluids – 1977. – Vol. 12. – P. 234.
18. H. Takabe, L. Montierth, R.L. Morse. Self□consistent eigenvalue analysis of Rayleigh–Taylor instability in an ablating plasma // Phys. Fluids – 1983. – Vol. 26. – P. 2299.
19. H.J. Kull. Incompressible description of Rayleigh–Taylor instabilities in laser□ablated plasmas //Phys. Fluids B – 1989. – Vol. 1. – P. 170.
20. R. Pakula, R. Sigel. Self□similar expansion of dense matter due to heat transfer by nonlinear conduction // Phys. Fluids – 1985. – Vol. 28. – P. 232.
21. G. Guderley. Starke kugelige und zylindrische verdichtungsstosse in der nahe des kugelmitterpunktes bnw. der zylinderachse // Luftfahrtforschung – 1942. – Vol. 19. – P. 302.
22. J. Sanz, J. A. Nicolás, J. R. Sanmartín, J. Hilario. Nonuniform target illumination in the deflagration regime: Thermal smoothing // Phys. Fluids – 1988. – Vol**.** 31**.** – P. 2320.